Supporting Information

Shen et al. 10.1073/pnas.0909181107

SI Text

Antibiotic Target Identification. Identification of unconditionally essential metabolic enzymes in *E. coli* MG1655 (Table S1).

Methods. Flux balance analysis and identification of unconditionally essential single enzymes of *E. coli* MG1655 metabolic network.

A reconstructed metabolic network consists of metabolites, metabolic reactions that convert these metabolites, and the metabolic enzymes that catalyze the metabolic reactions. The reconstructed metabolic network and biomass composition of *E. coli* MG1655 was obtained from its recent reconstruction, called iAF1260 (1), that contains 1260 enzymes, 2077 reactions, and 1039 metabolites. This reconstruction introduces another compartment (periplasm) in addition to cytoplasm and extracellular space and shows the exchange and transport reactions among these three compartments accordingly. The reconstructed metabolic network of *E. coli* MG1655 from (1) yields the stoichiometric matrix $\boldsymbol{S}$ with its element S_{ij} indicating the stoichiometric coefficient of metabolite i in reaction j. The FBA states that, in the stationary state, the fluxes $\{v_j\}$ of the metabolic reactions are those which maximize v_{biomass} subject to

$$\begin{aligned} &\boldsymbol{S}\cdot v = 0, \qquad v_j \geq 0 \qquad \text{for all irreversible reactions } j,\\ &v_j \leq v_{\max,j} \qquad \text{for all uptake reactions } j, \end{aligned} \qquad \textbf{[S1]}$$

where v_{biomass} indicates the flux of the reaction that produces biomass, acting as a drain of those biomass compounds. The biomass generating reaction is given by

$$\sum_i c_i m_i \rightarrow \text{biomass}$$

in which m_i is each of the biomass compounds and c_i is the coefficient. In calculating the unconditionally essential enzymes, first we run the calculation using both biomass compositions (wild-type and core) obtained in (1) and then consider only the enzymes that appear to be essential in both conditions.

For the FBA computations, we used ideally rich medium in which all the uptake reactions can occur without limitation on their fluxes, because we aim at identifying unconditionally essential enzymes, which we define below. The only exception was when the environment of the skin was considered. Here, due to the unique antimicrobial properties of the lipids on the skin surface (2), the fatty acid transporters were turned off.

The FBA is basically a linear programming problem, and we performed the analysis by using the GNU Linear Programming Kit. In the framework of the FBA, an enzyme is considered to be essential (1, 3) in a given environment if the constraint

$$v_j = 0 \qquad \textbf{[S2]}$$

for all reactions j catalyzed by an enzyme leads to zero flux of the biomass generating reaction

$$v_{\text{biomass}} = 0.$$

In the FBA scheme, the zero flux of the biomass generating reaction is interpreted as no growth of the organism. If such inactivation of an enzyme leads to no growth even in an ideally rich environment (medium) in which all the uptake reactions are allowed to occur without limitation, it would also lead to no growth in any other environment, and therefore we identify unconditionally essential—essential in all growth conditions—enzymes from the FBA [**S1**] combined with [**S2**] and setting all upper limits of uptake reactions to

$$v_{\max,j} = \infty \qquad \text{for all uptake reactions } j. \qquad \textbf{[S3]}$$

Structural and Evolutionary Analysis of FabD. ***Results.*** Structural and sequence conservation of a potential enzyme target among prokaryotes, and especially the conservation of its active site, is one prerequisite for broad-spectrum antibiotic development. A second prerequisite is that either no human ortholog exists for that enzyme, or that it is sufficiently different from its bacterial counterparts, in order to minimize potential drug toxicity. In humans, the elongation cycle enzymes are fundamentally different from their bacterial counterparts (4, 5). However, FabD exists in a cytosolic and mitochondrial form, the former playing the major role for fatty acid biosynthesis in human cells (4–6). For human mitochondrial FabD, a crystal structure is also available [Protein Data Bank (PDB) ID 2c2n]. Hence, we first performed a quantitative sequence homology search between *E. coli* FabD and the fifteen most common hospital isolates from the University of Pittsburgh Medical Center. We found that the bacterial enzymes' active sites show high amino acid sequence conservation (Fig. S1*A*), whereas the human mitochondrial enzyme has some critically different residues. Additionally, the human mitochondrial FabD active site showed the largest evolutionary distance compared to all examined bacterial species (Fig. S1*B*). Fig. S1*C* displays the *E. coli* FabD structure (*Right*) and its active site (*Left*), including catalytic and substrate binding residues and the bound substrate of the enzyme (malonate).

On a structural level, overall secondary structure of human FabDs showed similarity to its bacterial counterparts (see main text). However, a detailed structural comparison of the *E. coli* and human mitochondrial and cytosolic FabD active sites reveals sufficient differences between the human and prokaryotic enzymes to suggest that bacterial FabD may indeed serve as a useful molecular target for novel antibiotics. Furthermore, the potential surface analyses of these structures show that their charge distribution is different, especially at their active sites. Similar analyses can be performed for all bacterial target metabolic enzymes.

Potential Inhibitor Identification by Computational Chemistry. ***Methods and results.***

Docking and virtual screening.
Targets were identified as described in the main text and Fig. S2. The lead library of the ZINC database (7), containing approximately 10^6 commercially available small molecules prefiltered for drug-like properties (8), was screened by using Glide 4.5 (9, 10) The crystallographic structures for the enzymes involved in the different steps of the bacterial fatty acid pathway were downloaded from the Protein Database (see Table S2 for PDB codes of the crystal structures used for virtual screening as well as the known inhibitors for each enzyme). Homology models for *E coli* FabZ were built where necessary by using Prime (11) with the *P. falciparum* ortholog (PDB code 1z6b) as template. Solvent molecules and ligands were removed and Macromodel (12) atom types were assigned. Before the docking calculations, the protein and the ligands were preprocessed by using the protein preparation and ligprep modules of the Schrodinger 2007 Suite. For the

protein preparation, grid generation, and docking procedures, default Glide settings were used.

For each protein, the 10^5 top-ranked structures of the Glide high-throughput virtual screening were redocked at the single precision level, saving the 10^4 top-scored molecules. The resulting set was further screened by using the Glide extra precision scoring algorithm (Glide XP), retaining a database of 2,000 molecules. Fifty compounds of this database were selected on the basis of structural diversity, poses and scores, and significance of the interactions in the active site and further cross-docked by using GOLD (13). Fifteen compounds available commercially were selected for each protein for a more detailed evaluation of the free energy of binding by means of ensemble MM-PBSA calculations (see Table S3).

Molecular dynamics (MD) simulations.

To include protein flexibility into the rescoring of the putative ligands, MD simulations were performed for 15 FabD-ligand complexes and 26 FASII enzyme-ligands complexes. The SANDER.MPI module in the AMBER 9.0 (14) program package was used throughout the production simulations as well as for the minimization and equilibration protocols. Long-range interactions were handled by using the particle-mesh–Ewald summation (15). The SHAKE algorithm (12, 16) was employed on all atoms covalently bound to a hydrogen atom, allowing for an integration time step of 2 fs. Langevin dynamics (17) was used to control the temperature (300 K) by using a collision frequency of 1.0 ps^{-1}, with isotropic position scaling to maintain the pressure (1 atm). Initial atomic coordinates of each protein–ligand complex were taken from the pose derived from Glide XP docking. The complex was solvated in a periodic box of TIP3P (18) water molecules that extended 10 Å from the protein and was neutralized by Na^+ counterions by using the LEaP module (14, 19). The ff99 (20) and GAFF (21) force fields of AMBER 9 (14) were used to model the systems. Partial charges of the compounds were assigned by using the antechamber program in AMBER (RESP) (22–24), after geometry optimizations at the B3LYP/6-31G* level (25). For all MD simulations, 8-ns trajectories were computed after minimization and equilibration protein-compound systems. The trajectories were analyzed by using the PTRAJ module of AMBER.

Binding free energy calculations using Ensemble MM-PBSA.

The MM-PBSA approach represents the postprocessing method to evaluate free energies of binding, combining molecular mechanical energies with continuum solvent approaches (26, 27). It has been demonstrated to significantly improve correlation with experimental binding constants (28, 29). The PBSA module of Amber 9 has been used in all cases with default parameters. Snapshots of the protein, small molecule ligand, and complex were extracted every 10 ps from the last 4 ns of each MD trajectory. The electrostatic contribution to the solvation free energy was calculated by solving the PB equation in MM-PBSA (30). The hydrophobic interaction term was derived from the solvent-accessible-surface-area-dependent term (31). The entropy term was neglected, assuming that it is similar when similar compounds bind to the same protein, and will not affect differences in binding energies.

Inhibitor fits into the active site of enzymes.

Ten out of 26 tested FASII elongation cycle potential inhibitors showed activity in the in vitro elongation assay. There is at least one active inhibitor for each of the seven elongation enzymes. The results and poses for ECi8 (targeting FabB/F), ECi16 (inhibiting FabI), and ECi23 (targeting FabZ) were already discussed in the main text. Here we report the binding modes of the other 7 active compounds (Figs. S3 and S4), including three predicted FabH inhibitors (ECi11, ECi12, and ECi26), one FabB/F inhibitor (ECi21), one FabG inhibitor (ECi10), one FabA inhibitor (ECi13), and one FabI inhibitor (ECi14).

Enzyme Assays, Bacterial Viability, and Toxicity Studies. *Methods and results.*

In vitro enzyme assays.

Materials and reagents.

Malonyl–CoA, CoA, BSA, NADP, NADPH, KDH (porcine heart), α-ketoglutaric acid, TPP, Cerulenin, Triclosan, MTT, and IPTG were purchased from Sigma. EDTA, TCEP, and DMSO were obtained from Fluka. DMEM, glutamine, sodium pyruvate, phenol red, pET-151 vector, and *E. coli* BL21 and Top10 competent cells were obtained from Invitrogen. The agarose gel-extraction kit and the plasmid DNA isolation kit were purchased from Qiagen. The FabD inhibitors and elongation cycle inhibitors were purchased from ChemBridge, ChemDiv, and Ryan Scientific. HisTrap FF columns were obtained from GE Healthcare. Bradford reagents and Coomassie blue were purchased from Bio-Rad.

FabD enzyme assay and the screening of potential FabD inhibitors.

Purification of his-FabD and his-holo-ACP: *E. coli* FabD was amplified from the genomic DNA of *E. coli* MG1655 strain by using PCR and cloned into the pET151-TOPO vector from Invitrogen. Plasmids, pDSNdeIacpPec, and pDSNdeIacpSec, containing the coding sequence for *E. coli.* AcpP and AcpS, respectively, were generous gifts from Dr. Roland Lange (Actelion Pharmaceuticals Ltd., Switzerland). pET-151-fabD or pDSNdIcpPEc and pDSNdeIacpSEC were transformed or cotransformed into competent *E. coli* Top10 cells (Invitrogen). *E. coli* his-FabD and his-holo-ACP were overexpressed in *E. coli* BL21 cells induced with 0.5 mM IPTG at 37 °C for 3 hours. Cells were then harvested by centrifugation and stored at −80 °C. The bacterial cell pellet was resuspended in the lysis buffer and disrupted by sonication. After centrifugation, the supernatant was filtered and applied to the AKTA system (GE Healthcare) by using HisTrap FF column. The FabD-containing fractions were then pooled, concentrated, and equilibrated in the enzyme assay buffer (50 mM phosphate buffer, pH 6.8, 1 mM EDTA, 1mM DTT). The protein concentration of his-FabD and his-holo-ACP was determined by Bradford assays.

Fluorometric coupled FabD enzyme assay.

The FabD enzyme assay was performed as described previously (32) with minor modifications. Briefly, 46 μL 0.06 nM his-FabD solution (50 mM phosphate buffer, pH 6.8, 1 mM EDTA, 1 mM DTT, and 0.1 mg/mL BSA) was preincubated with 4 μL 10 μg/μL of the 15 different predicted FabD small molecule inhibitors or DMSO for 30 min at 28 °C. To start the reaction, 25 μL ACP/KDH mix (240 μM his-ACP, 8 mM α-ketoglutaric acid, 1 mM NAD, 60 mU/100 μL KDH, and 0.8 mM TPP) and 25 μL Malonyl-CoA solution (100 μM Malonyl-CoA in 50 mM phosphate buffer, pH 6.8, 1 mM EDTA, 1 mM DTT) were added. NADH-dependent fluorescence was immediately measured for a minimum of 5 min by using a microtiter plate reader (Beckman Coulter DTX880) equipped with an excitation filter at 340 nm (bandwidth 20 nm) and an emission filter at 465 nm (bandwidth 35 nm). The fluorescence signal was set to an integration time of 1 s (no lag time) and three flashes per well. The experiments were run at 28 °C in triplicates.

Fluorometric KDH counter screening assays.

The KDH assay was performed as follows: 3.75 mU KDH was diluted in 75 μL 50 mM phosphate buffer, pH 6.8, 1 mM EDTA, 1 mM DTT, 2.67 mM α-ketoglutaric acid, 0.33 mM NAD, and 0.267 mM TPP and added to 4 μL DMSO (controls) or 10 μg/μL inhibitors dissolved in DMSO. A 60 μM CoA solution

was prepared in 50 mM phosphate buffer, pH 6.8, 1 mM EDTA, 1 mM DTT. All solutions and the microplate reader were prewarmed at 28 °C; 21 μL CoA solution was added to start the reactions that were measured immediately over 5 min in triplicates.

Elongation cycle assay and the screening of potential inhibitors. We utilized an established elongation assay for type-II fatty acid synthesis (33) with slight modifications. Briefly, *E. coli* MG1655 was grown to a stationary phase in LB medium. The cultures were centrifuged and the pellets were washed and lysed in ice-cold buffer. The supernatants were then precipitated by using ammonium sulfate. The 45–80% ammonium sulfate saturated protein fraction which contained all the FASII enzymes was dialyzed. Subsequently, 2–16 μg cell lysate was first incubated with different concentrations of inhibitors at 37 °C for 20 min in 50 μL buffer containing 5 mM EDTA, 1 mM NADPH, 1 mM NADH, 5 mM β-mercaptoethanol, 150 μM DTT, 16 μM ACP (pretreated with 3 mM ice-cold DTT for 20 min), 40 μM acetyl-CoA, 4% DMSO, and 100 mM sodium phosphate (pH 7.0). Then 120 μM 10 μl malonyl-CoA was added into the 50-μL solution to initiate the reaction. After 30 minutes reaction at 37 °C, 60 μL of each sample (plus 15 μL 5X native sample buffer) were applied to a 16% polyacrylamide gel containing 0.5 M urea (to separate intermediate and final products) or 4 M urea (to separate different chain lengths of acyl-ACP products). After electrophoresis, the gels were stained with Coomassie blue for visualization. Reactions with no inhibitor (only DMSO) were used as negative controls. Known FASII elongation cycle inhibitors triclosan (167 μg/mL) and thiolactomycin (167 μg/mL) were used as positive controls.

In vitro enzyme assay results. Five inhibitors completely block the enzymatic activity of FabD (yellow shading) and generate negatively changing fluorescence signals (NADH), whereas the three weak inhibitors (orange shading) can significantly decrease the rate of fluorescence signals catalyzed by the purified FabD's activity compared to that in the presence of DMSO or the absence of inhibitors (see Table S4). Because the established FabD enzyme assay (32) was based on the FabD-KDH coupled reactions, we also performed a KDH counterscreening assay to eliminate the possible inhibition of potential inhibitors against KDH. FDi11, 12, 14, and 15 did not show any inhibition against KDH compared to DMSO control, whereas FDi2, 7, 8, and 10 can partially inhibit the KDH activity. However, the partial inhibition of fluorescence signals catalyzed by the KDH enzyme in the presence of FDi 2, 7, 8, and 10 could also be attributed to the direct destruction of NADH by the inhibitors. The strong negative slope suggests this possibility for the case of FDi7. Nevertheless, FDi2, 7, 8, 10, 11, 12, 14, and 15 could still be the potential inhibitors against FabD activity in vitro as indicated by the whole cell assays.

As shown in Fig. S5, with no inhibitors (only DMSO) present, the FASII elongation cycle proceeds normally and generates long chain acyl-ACPs, showing only the unreacted substrate ACP as well as the product acyl-ACP in the gel. Inhibitors should cause the accumulation of the substrates of their enzyme targets; for example, triclosan (34) mainly accumulates the substrate of FabI: C4:1(Δ2)-ACP, and cerulenin (34) causes major accumulation of the substrate of FabB/F: C4:0-ACP. Among the tested compounds, ECi8 gives the strongest inhibition, which causes a significant reduction in the acyl-ACP band. ECi16 also has notable activity, whereas ECi11 shows slight activity. ECi8, which was predicted as an inhibitor for FabB and FabF, generated a similar pattern as triclosan. This implies that ECi8 might also inhibit FabI, which is in agreement with the cross-docking results that ECi8 has a reasonable docking pose in the open conformation of FabI. ECi8, ECi21, ECi23, and ECi26 show at least some inhibition toward FASII enzymes. ECi26 leads to a notable accumulation of malonyl-ACP, which is the substrate of its predicted protein target: FabH. ECi22 seems to decompose the cell lysate. By comparison of the acyl-ACP bands to the DMSO control, ECi10, ECi11, ECi12, ECi13, ECi14, and ECi16 display weak inhibition. ECi8 inhibits FASII enzymes in a dose-dependent manner instead of nonspecific aggregation-based inhibition. In total, 10 out of 26 predicted FASII elongation cycle inhibitors showed activity in the in vitro elongation assay by causing the reduction of acyl-ACP production. There is at least one active inhibitor for each of the seven elongation enzymes.

In vivo viability and toxicity assays.

Bacterial disc inhibition assay. The disc inhibition assay was performed as described previously (35). Briefly, freshly grown *E. coli* (MG1655 strain and patient strain) and *S. aureus* (Mu50 strain, USA300 strain, and patient strain) cultures ($OD_{600} = 0.3$) were evenly inoculated onto the surface of LB or LB plus 10% human serum agar plates. Sterile filter discs soaked with 10 μL of 10 mg/mL of the different inhibitors were then applied to the surface of the inoculated plates and incubated for 16–20 h at 37 °C. We used 1 mg/ml Ampicillin and 10 μL DMSO as positive and negative controls, respectively.

MTT cell viability assay. Cell viability was determined by 3-[4,5-dimethyl-triazolyl-2]2, 5-diphenyl tetrazolium bromide (MTT) assay. The human BJ fibroblast cells expressing hTERT (CL1 cells) (36) were seeded in 24-well plates at a density designed to reach 90% confluence at the time of assay. The next day, the culture medium was replenished with fresh medium with 400 μg/mL of the potential inhibitors. The same amount of DMSO was used as a control. After 24 h of inhibitor treatment, MTT was added to a final concentration of 0.5 mg/mL, and the plate was incubated for 3 h at 37 °C. Cells having functional mitochondrial succinate dehydrogenase can convert MTT to formazan that generates a blue color when dissolved in DMSO. The absorbance was read at 540 nm by using a plate reader (Beckman DTX880).

Trypan blue exclusion assay. CL1 cells were seeded at a density of 1×10^5 cells in 12-well plates and cultured in DMEM (25 mM glucose, 4 mM glutamine) containing 10% FBS at 37 °C in an incubator with 5% CO_2 and 95% air. The next day, the culture medium was replenished with fresh medium with 400 μg/mL of the inhibitors. The same amount of DMSO was used as a control. After 24 h of inhibitor treatment, the cells were harvested by releasing them with 0.05% trypsin and 0.53 mM EDTA, stained with trypan blue, and counted. Cell counting data were determined by blinded counting of both live (unstained) and dead (blue) cells on a standard grid-patterned hemocytometer. The mean number of cells and the standard deviation of the mean were determined, and data were then compared by using a standard Student *t* test to determine statistically significant differences between cell populations.

In vivo viability and toxicity results. The in vitro and in vivo effects of the predicted small molecule inhibitors were summarized in Table S5.

1. Feist AM, et al. (2007) A genome-scale metabolic reconstruction for Escherichia coli K-12 MG1655 that accounts for 1260 ORFs and thermodynamic information. *Mol Syst Biol* 3:121.
2. Drake DR, Brogden KA, Dawson DV, Wertz PW (2008) Antimicrobial lipids at the skin surface. *J Lipid Res* 49:4–11.
3. Lee D-S, et al. (2009) Comparative genome-scale metabolic reconstruction and flux balance analysis of multiple Staphylococcus aureus genomes identify novel antimicrobial drug targets. *J Bacteriol* 191:4015–4024.
4. Campbell JW, Cronan JE (2001) Escherichia coli FadR positively regulates transcription of the fabB fatty acid biosynthetic gene. *J Bacteriol* 183:5982–5990.

5. Maier T, Leibundgut M, Ban N (2008) The crystal structure of a mammalian fatty acid synthase. *Science* 321:1315–1322.
6. Heath RJ, Rock CO (2004) Fatty acid biosynthesis as a target for novel antibacterials. *Curr Opin Investig Drugs* 5:146–153.
7. Irwin JJ, Shoichet, BK (2005) ZINC—A free database of commercially available compounds for virtual screening. *J Chem Inf Model* 45:177–182.
8. Teague SJ, Davis AM, Leeson PD, Oprea T. (1999) The design of leadlike combinatorial libraries. *Angew Chem Int Ed Engl* 38:3743–3748.
9. Friesner RA, et al. (2004) Glide: A new approach for rapid, accurate docking and scoring. 1. Method and assessment of docking accuracy. *J Med Chem* 47:1739–1749.
10. Friesner RA, et al. (2006) Extra precision glide: Docking and scoring incorporating a model of hydrophobic enclosure for protein-ligand complexes. *J Med Chem* 49:6177–6196.
11. Zhu K, Shirts MR, Friesner RA (2007) Improved methods for side chain and loop predictions via the protein local optimization program: Variable dielectric model for implicitly improving the treatment of polarization effects. *J Chem Theory Comp* 3:2108–2119.
12. Macromodel. (2007) version 9.5; Schrödinger, LLC: New York.
13. Verdonk ML, Cole JC, Hartshorn MJ, CW M, Taylor RD (2003) Improved protein-ligand docking using GOLD. *Proteins* 52:609–623.
14. Case DA, et al. (2006) University of California, San Francisco.
15. Essman V, et al. (1995) A smooth particle-mesh-Ewald method. *J Chem Phys* 103:8577–8593.
16. Ryckaert JP, Ciccotti G, Berendsen HJC (1977) Numerical integration of the Cartesian equations of motion of a system with constraints: Molecular dynamics of n-alkanes. *J Comput Phys* 23:327–341.
17. Pastor RW, Brooks BR, Szabo A (1988) An analysis of the accuracy of Langevin and molecular dynamics algorithms. *Mol Phys* 65:1409–1419.
18. Jorgensen WLC, Madura J, Impey RW, Klein ML (1983) Comparison of simple potential functions for the simulation of liquid water. *J Chem Phys* 79:926–935.
19. Schafmeister C, Ross WS, Romanovski V (1995) University of California, San Francisco.
20. Cieplak P, Caldwell J, Kollman P (2001) Molecular mechanical models for organic and biological systems going beyond the atom centered two body additive approximation: Aqueous solution free energies of methanol and n-ethyl acetamide, nucleic acid base, and amide hydrogen bonding and chloroform/water partition coefficients of the nucleic acid bases. *J Comput Chem* 22:1048–1057.
21. Wang J, Wolf RM, Caldwell JW, Kollman PA, Case DA (2004) Development and testing of a general AMBER force field. *J Comput Chem* 25:1157–1174.
22. Bayly CA, Cieplak P, Cornell WD, Kollman PA (1993) A well behaved elestrostatic potential based method using charge restraints for deriving atomic charges: The RESP model. *J Phys Chem* 97:10269–10280.
23. Fox T, Kollman PA (1998) Application of RESP methodology in the parametrization of organic solvents. *J Phys Chem B* 102:8070–8079.
24. Pearlman DA, et al. (1995) *Comput Phys Commun* 91:1.
25. Becke AD, Yarkony DR (1995) *Modern Electronic Structure Theory Part II* (World Scientific, Singapore).
26. Gohlke H, Case DA (2003) Converging free energy estimates: MM-PB(GB)SA studies on the protein–protein complex ras–raf. *J Comput Chem* 25:238–250.
27. Wang J, Morin P, Wang W, Kollman P (2001) Use of MM-PBSA in reproducing the binding free energies to HIV-1 RT of TIBO derivatives and predicting the binding mode to HIV-1 RT of Efavirenz by docking and MM-PBSA. *J Am Chem Soc* 123:5221–5230.
28. Guimaraes CRW, Cardozo M (2008) MM-GB/SA rescoring of docking poses in structure-based lead optimization. *J Chem Inf Model* 48:958–970.
29. Thompson DC., Humblet C, Joseph MD (2008) Investigation of MM-PBSA rescoring of docking poses. *J Chem Inf Model* 48:1081–1091.
30. Onufriev A, Bashford D, Case DA (2000) *J Phys Chem B* 104:3712–3715.
31. Sitkoff D, Sharp KA, Honig B (1994) *J Phys Chem* 98.
32. Molnos J, Gardiner R, Dale GE, Lange R (2003) A continuous coupled enzyme assay for bacterial malonyl-CoA:acyl carrier protein transacylase (FabD). *Anal Biochem* 319:171–176.
32. Kodali S, Galgoci A, Singh SB, Wang J (2006) Gel-elongation assay for type II fatty acid synthesis. *Nature Protocols* DOI:10.1038/nprot.2006.1134.
34. Zhang YM, White SW, Rock CO (2006) Inhibiting bacterial fatty acid synthesis. *J Biol Chem* 281:17541–17544.
35. Woods GL, Washington JA (1995) in *Manual of Clinical Microbiology*, eds Murray PR, Baron EJ, Pfaller MA, Tenover FC, Yolken RH (ASM, Washington, DC).
36. Hahn WC, et al. (1999) Creation of human tumour cells with defined genetic elements. *Nature* 400:464–468.

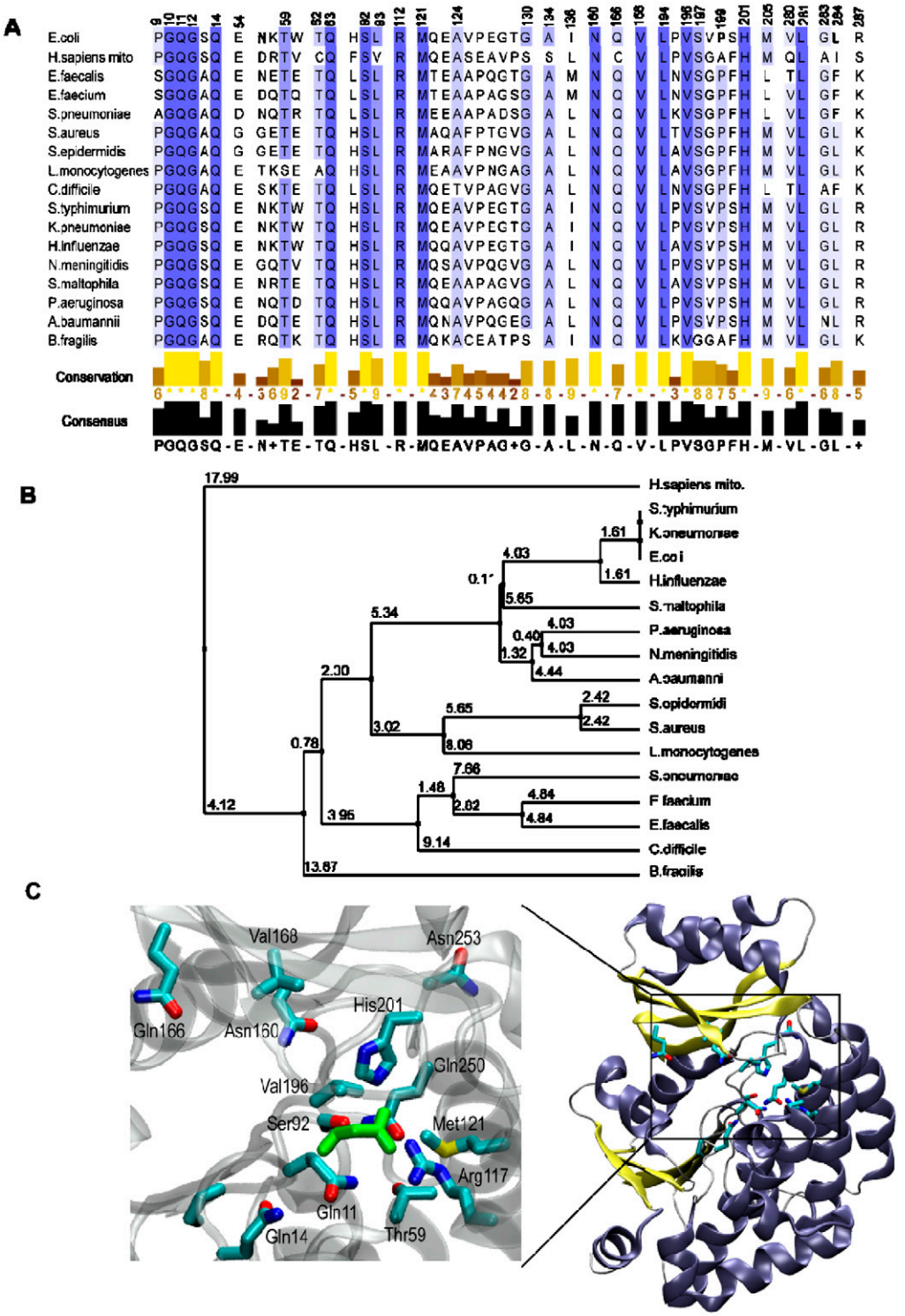

Fig. S1. Comparison of FabD sequence and structure between human mitochondrial and the 16 most common bacterial pathogens (among hospital isolates). (*A*) Sequence similarities of the FabD active sites. The residues lining the active site of FabD of human mitochondria and the bacterial species show some distinct features. The residues are labeled with their corresponding residue numbers in *E. coli* FabD. The *Middle* shows the conservation score for each residue. Stars indicate full conservation among all species. The *Bottom* shows the most common residues in the active sites. (*B*) Evolutionary distance of FabDs. The phylogenetic tree shows the evolutionary relationships among pathogenic bacteria with existing FabD sequence and human mitochondrial FabD. The numbers on the tree branches indicate the average distance measured in sequence identity. (*C*) The structure of *E. coli* FabD. The *Right* shows the ribbon diagram of *E. coli* FabD, whereas the *Left* is a closer look at its active site. Catalytic and substrate binding residues are displayed and labeled. A bound substrate of the enzyme (malonate) is shown in green. PDB IDs that are used for the figure are 1mla, 2g2y, 2g2z.

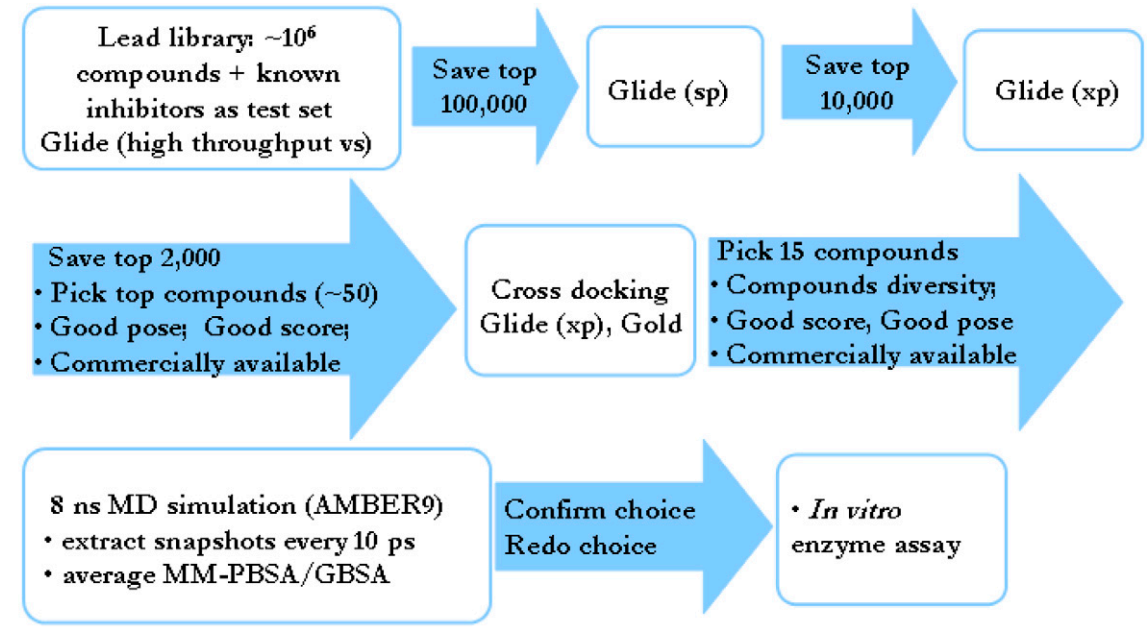

Key points of virtual screening protocol:

- Retrieval or homology modeling of identified target enzymes
- Virtual screening of 10^6 compounds for each target
- Cross-docking with multiple scoring functions
- MM-PBSA Ensemble rescoring of selected candidates

Fig. S2. Procedure for docking and virtual screening of FASII enzymes.

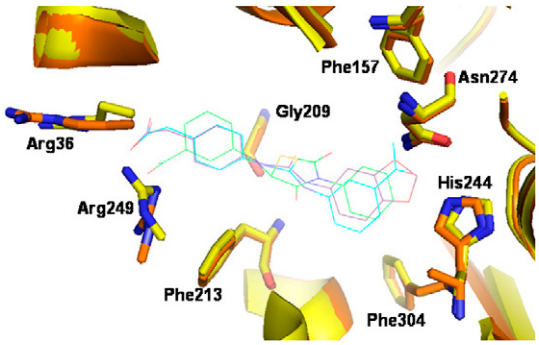

Fig. S3. Docking poses of active FabH inhibitors in two different *E. coli* FabH crystal structures (PDB codes 1hnd and 2eft) with different flexible side chains such as Arg 36 and Arg249. The active site of FabH is not very flexible, and there are no large domain movements or loop movement upon ligand binding, as indicated by the comparison with the two crystal structures with and without a ligand. However, in the mouth of the FabH active site there are several flexible arginines with different conformations in the presence of different inhibitors. To account for the side chain flexibility of proteins, we performed virtual screening on the basis of multiple enzyme structures and select compounds that have reasonable interactions with the different enzyme structures. ECi11 (purple) and ECi12 (cyan) were docked to 1hnd (yellow), whereas ECi26 (green) to 2eft (orange). ECi11 and ECi12 have very similar scaffolds. Their carboxylate groups form salt-bridge interactions with Arg36 and Arg249. The two NH (-NHCSNH-) moieties form hydrogen bonds with Gly209. They also form hydrogen bonds with two active-site conserved residues Asn274 and His244. ECi26 has a different scaffold. It has three rings and a better shape fitting to the active site. It forms a salt bridge with Arg249 in the mouth of the active site similar to ECi11 and ECi12. It also forms a hydrogen bond with Phe213. The phenyl ring in ECi26 stacks against Phe304 inside the active site, but there are no hydrogen bonds with Asn274 or His244.

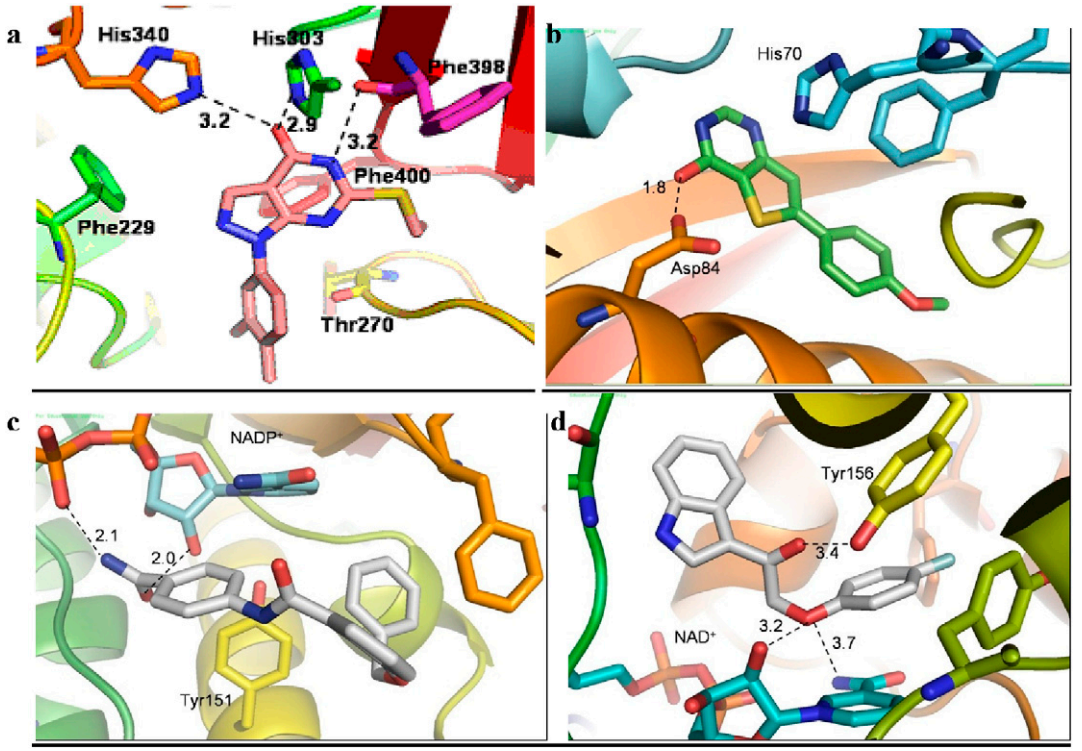

Fig. S4. Selected active compounds identified from FASII elongation assay and docking poses in their respective enzyme targets. (*A*) ECi21 docked in *E. coli* FabF crystal structure (PDB: 2gfx) predicted as a FabB/F inhibitor. ECi21 has a binding mode similar to both thiolactomycin and platensimycin. It makes critical interactions with the catalytic residues in the active site of FabB/F. Its carbonyl oxygen group forms hydrogen bonds with His^{340} and His^{303}. It also makes a hydrogen bond with Phe^{398}. Its ring forms favorable π-stacking with the gate-keeping residue Phe^{400}. It fits well in the malonyl-ACP pocket. (*B–D*) The interactions shown in (*B*) for ECi13 docked in *E. coli* FabA (predicted as a FabA inhibitor) reinforce the relevance of Asp^{84} in FabA inhibition, already discussed for FabZ (see Fig. 2*G*); (*C*) ECi10 docked in *E. coli* FabG, predicted as a FabG inhibitor; (*D*) ECi14 docked in *E. coli* FabI, predicted as a FabI inhibitor. Similarly to ECi10, the interactions of ECi14 in the active site of FabI resemble those described for ECi16 (Fig. 2*F*). As for the case of FabG, Tyr^{151} and the NADP+ cofactor are the main players in ligand binding to the FabG active site (*C*). A scaffold with phenyl rings connected by a polar moiety characterizes the FabI and FabG inhibitors, because the aromatic portions are stabilized by stacking interactions with the oxidized nicotinamide of the cofactor and Phe and Tyr residues close to the active site, whereas the polar group facilitates hydrogen bond interactions.

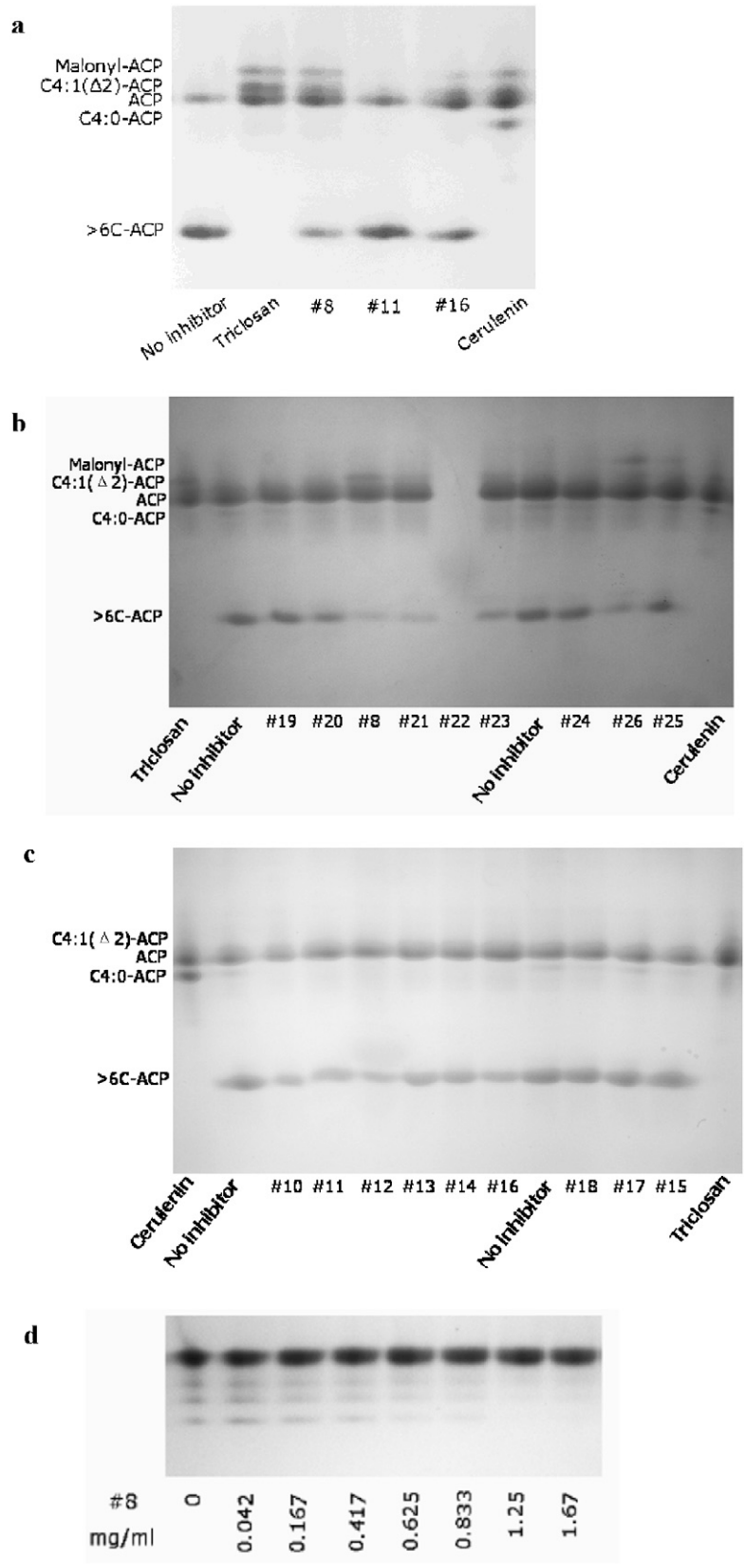

Fig. S5. Representative results for the FASII elongation cycle inhibition assay. (*A*) Modified elongation assay in the presence of putative elongation cycle enzyme inhibitors: ECi8, ECi11, and ECi16 (833 μg/mL) incubated with 8 μg *E. coli* cell lysate. (*B*) ECi8, ECi19, ECi20, ECi21, ECi22, ECi23, ECi24, ECi25, and ECi26 (833 μg/mL) were tested against 4 μg cell lysate. (*C*) ECi10, ECi11, ECi12, ECi13, ECi14, ECi15, ECi16, ECi17, and ECi18 (833 μg/mL) were tested against 16 μg cell lysate. (*D*) Dose-dependent inhibition of ECi8 toward FASII elongation enzymes (4 μg *E. coli* cell lysate).

Table S1. Predicted essential enzymes using flux balance analysis (FBA) method based on reconstructed *E. coli* K-12 MG1655 metabolic network (1)

	Gerdes	Baba	Kang			Gerdes	Baba	Kang
aldA					hemH			
aroA					hemL			
aroC					ispA			
cmk					metK			
coaA					mraY			
coaD					mtn			
coaE					murA			
dfp					murB			
folC					nadK			
folE					ndk			
folP					plsB			
glmM					plsC			
glmU					psd			
gltX					pssA			
gmk					ribD			
hemB					ribF			
hemD					serC			
hemE					thiL			
hemG					tmk			

LLThe list of essential enzymes of *E. coli* K-12 MG1655 predicted by FBA analysis is shown. Red indicates uniform agreement with three genome-scale *E. coli* viability studies, black represents one or two mismatches, and green indicates disagreement with all 3 *E. coli* viability studies. Background of orange (gray) indicates the gene is identified as essential (nonessential) in the given *E. coli* deletion phenotype analysis (2–4).

Table S2. Crystal structures or homology models of the FASII enzymes used for virtual screening as well as known inhibitors for each enzyme

Enzyme	Avail PDBs & homology model (organism)	Known inhibitors
FabB	2aqb (*E. coli*) with thiolactomycin analog, 2.19 Å; 2vb8 (*E. coli*) with thiolactomycin, 1.52 Å	Thiolactomycin, Cerulenin, Platencimycin,
FabF	2gfx (*E. coli*) with platensimycin, 2.59 Å, C163Q mutate back; 2gfv (*E. coli*) 2.29 Å, C163Q mutate back; 2gqd (*S. aureus*) 2.3 Å	Platencin, BABX, Phomallenic acids
FabH	1hnj (*E. coli*) with malonyl coenzyme A, 1.46 Å; 1hnd (*E. coli*) with coenzyme A, 1.6 Å; 1mzs (*E. coli*) with indole analog, 2.1 Å; 2eft (*E. coli*) with coenzyme A, 2.0 Å; 1zow (*S. aureus*) 2.0 Å	HR12, Indole analogs, Platencin, 1,2-Dithiole-3-ones, Benzoylaminobenzoic acids
FabD	2g2y (*E. coli*) with malonic acid, 2.26 Å; 2g2z (*E. coli*) with coenzyme A & malonic acid, 2.8 Å; 1mla (*E. coli*) 1.5 Å; *S. aureus* homology model built based on *E. coli* 2g2y (39% similarity)	Corytuberine
FabG	1q7b (*E. coli*) with NADP+, 2.05 Å; 1q7c (*E. coli*) with NADPH, 2.50 Å,Y157F mutant, mutated back	Polyphenols, flavones
FabI	1qg6 (*E. coli*) with NAD & triclosan, 1.9 Å; 1mfp (*E. coli*) with NAD & SB611113, 2.33 Å; 1dfh (*E. coli*) with NAD & thieno azaborine, 2.2 Å	Diazaborines, Diphenyl ethers, Triclosan, Isoniazid, Aminopyridines, Polyphenols
FabA	1mka (*E. coli*) 2 Å;	Allenic acids, 3-Decynoyl-NAC
FabZ	*E. coli* homology model built based on *P. falciparum* 1z6b 2.1 Å (45% similarity)	NAS-91, NAS-21

Table S3. Structures of compounds showing activity in in vitro experiments

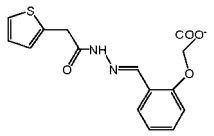

FDi2
ZINC00725132g2y
GScore: −6.09
MMPBSA: −41.56

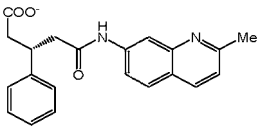

FDi4
ZINC001527932g2y
GScore: −9.94
MMPBSA: −42.61

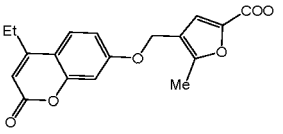

FDi7
ZINC002009292g2y
GScore: −8.18
MMPBSA: −52.72

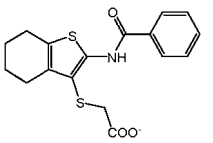

FDi8
ZINC002842752g2y
GScore: −12.27
MMPBSA: −33.51

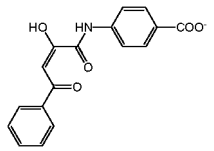

FDi10
ZINC029683912g2y
GScore: −10.5
MMPBSA: −34.22

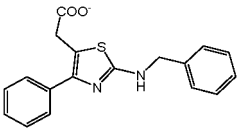

FDi11
ZINC033507622g2y
GScore: −7.28
MMPBSA: −40.94

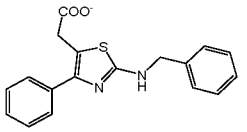

FDi12
ZINC036602992g2y
GScore: −8.54
MMPBSA: −31.81

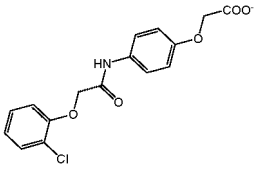

FDi14
ZINC048196752g2y
GScore: −7.94
MMPBSA: −18.89

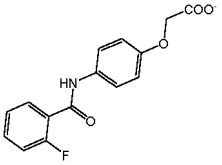

FDi15
ZINC067022822g2y
GScore: −7.35
MMPBSA: −31.07

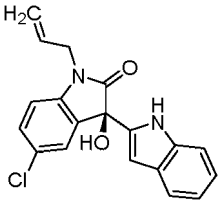

ECi8
ZINC022148252gfv
GScore: −11.67
MMPBSA: −32.52

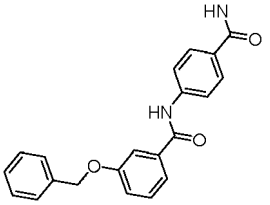

ECi10
ZINC066976421q7b
GScore: −9.10
MMPBSA: −25.67

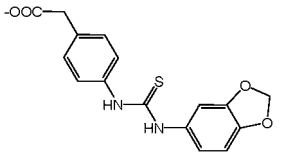

ECi11
ZINC046181811hnj
GScore: −10.52
MMPBSA: −34.24

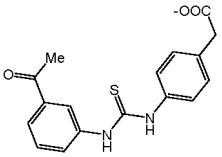

ECi12
ZINC006214611hnj
GScore: −11.36
MMPBSA: −31.84

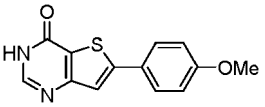

ECi13
ZINC047163541mka
GScore: −12.98
MMPBSA: −23.7

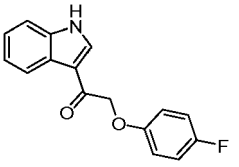

ECi14
ZINC044872831qg6
GScore: −13.8
MMPBSA: −28.3

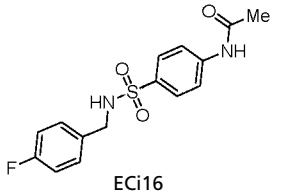

ECi16
ZINC004331161qg6
GScore: −13.42
MMPBSA: −36.71

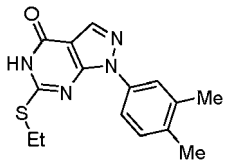

ECi21
ZINC049284622gfx
GScore: −11.03
MMPBSA: −37.35

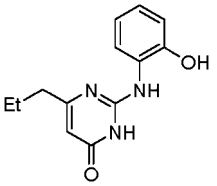

ECi23
ZINC01281455Homolog
built on 1z6b
GScore: −15.07
MMPBSA: −42.84

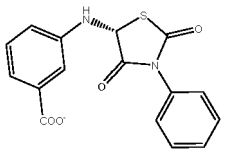

ECi26
ZINC013179351hnj
GScore: −8.38
MMPBSA: −40.79

LLThis table includes the numbering of the compounds used in the study, their corresponding ZINC numbers, the PDB number of the crystal structures used to screen against in the computational studies, Gscore (kcal/mol) from docking using Glide XP, and MM-PBSA score (kcal/mol) from MM-PBSA calculation on the basis of 8-ns molecular dynamics simulation using Amber 9.

Table S4. Summary of the in vitro enzyme assays of FabD inhibitors

	FabD assay			KDH assay
Slopes	1	2	3	
Control	40.856	34.51	40.1925	-
DMSO	30.972667	31.410333	35.731	-
FDi1	32.251	29.645	30.805	**N/A**
FDi2	-13.557	-10.892	-17.063	±
FDi3	23.044	26.97	23.515	**N/A**
FDi5	25.257	26.247	21.728	**N/A**
FDi6	23.515	26.285	22.732	**N/A**
FDi7	-575.525	-401.568	-623.088	±
FDi8	-4.537	-8.743	-7.943	±
FDi9	22.597	25.545	24.113	**N/A**
FDi10	1.492	2.375	1.615	±
FDi11	2.292	-8.643	-17.61	-
FDi12	18.667	15.572	19.612	-
FDi13	23.272	31.678	22.952	**N/A**
FDi14	21.112	24.532	19.297	-
FDi15	16.681	18.493	14.22	-

LLStrong inhibitors (yellow shading) and weak inhibitors (orange shading) are shown. +++: Strong inhibition; ±: partial inhibition; –: no inhibition in KDH counterscreening.

Table S5. Summary of the in vitro and in vivo effects of the predicted small molecule inhibitors

				Enzyme assay		Disc inhibition assay		
#	ZINC #	Predicted targets	Elongation assay	FabD-KDH	KDH	*E. coli*	*S. aureus*	Cell toxicity assay
FDi1	00037017	FabD		–				
FDi2	00072513	FabD		++	+	+	+	–
FDi3	00118785	FabD		–				
FDi4	00152793	FabD		++	++	–	–	
FDi5	00152819	FabD		–				
FDi6	00155674	FabD		–				
FDi7	00200929	FabD		++	+	+	++	+
FDi8	00284275	FabD		++	+	–	–	
FDi9	00615908	FabD		–				
FDi10	02968391	FabD		++	+	+	++	+
FDi11	03350762	FabD		++	–	–	–	
FDi12	03660299	FabD		+	–	–	–	
FDi13	04325226	FabD		–				
FDi14	04819675	FabD		+	–	+	+	+
FDi15	06702282	FabD		+	–	–	–	
ECi1	00530522	FabB&FabF	–					
ECi2	04003094	FabB&FabF	–					
ECi3	00270140	FabG	–					
ECi4	06706704	FabG	–					
ECi5	00616124	FabI	–					
ECi6	00621174	FabI	–					
ECi7	00451671	FabG	–					
ECi8	02214825	FabB&FabF	++			+	++	++
ECi9	00318243	FabI	–					
ECi10	06697642	FabG	+			–	–	
ECi11	04618181	FabH	+			–	–	+
ECi12	00621461	FabH	+			–	–	
ECi13	04716354	FabA	+			–	–	
ECi14	04487283	FabI	+			–	–	
ECi15	00450024	FabB&FabF	–			–	–	
ECi16	00433116	FabI	+			+	–	+
ECi17	00162806	FabH	–					
ECi18	04389413	FabH	–					
ECi19	05138705	FabH	–					
ECi20	05011121	FabB&FabF	–					
ECi21	04928462	FabB&FabF	++			–	–	
ECi22	00215652	FabZ	Decompose					
ECi23	01281455	FabZ	++			+	+	++
ECi24	00429948	FabI	–					
ECi25	06753074	FabH	–					
ECi26	01317935	FabH	++			–	–	
Triclosan		FabI	++			++	++	++
Cerulenin		FabB&FabF	++			++	++	++

LLThe table contains the numbering of inhibitors used in the studies, their corresponding ZINC number from ZINC database, their predicted targets on the basis of virtual screening, the result from FabD-KDH coupled assay and KDH assay (see Table S4 for more detail), or FASII elongation assay (see Fig. S5 for more details), the result from the disc inhibition assay on a LB agar plate, and the cytotoxicity assays.
++: Strong activity; +: weak activity; –: inactive; empty: no experimental data.